Catalytic Stimulation by Restrained Active-Site Floppiness—The Case of High Density Lipoprotein-Bound Serum Paraoxonase-1

ARTICLE *in* JOURNAL OF MOLECULAR BIOLOGY · JANUARY 2015

Impact Factor: 4.33 · DOI: 10.1016/j.jmb.2015.01.013

6 AUTHORS, INCLUDING:

Moshe Ben-David
Weizmann Institute of Science
7 PUBLICATIONS **244** CITATIONS
SEE PROFILE

Joel Sussman
Weizmann Institute of Science
359 PUBLICATIONS **22,732** CITATIONS
SEE PROFILE

Christopher Maxwell
Uppsala University
15 PUBLICATIONS **204** CITATIONS
SEE PROFILE

Shina Caroline Lynn Kamerlin
Uppsala University
61 PUBLICATIONS **1,579** CITATIONS
SEE PROFILE

Catalytic Stimulation by Restrained Active-Site Floppiness—The Case of High Density Lipoprotein-Bound Serum Paraoxonase-1

Moshe Ben-David[1,2], Joel L. Sussman[1], Christopher I. Maxwell[3], Klaudia Szeler[3], Shina C.L. Kamerlin[3] and Dan S. Tawfik[2]

*1 - **Department of Structural Biology,** Weizmann Institute of Science, Rehovot 76100, Israel*
*2 - **Department of Biological Chemistry,** Weizmann Institute of Science, Rehovot 76100, Israel*
*3 - **Science for Life Laboratory,** Department of Cell and Molecular Biology, Uppsala University, S-754 21 Uppsala, Sweden*

***Correspondence to Shina C.L. Kamerlin and Dan S. Tawfik:** S. C. L. Kamerlin is to be contacted at kamerlin@icm.uu.se; D. S. Tawfik is to be contacted at tawfik@weizmann.ac.il. kamerlin@icm.uu.se; tawfik@weizmann.ac.il*
http://dx.doi.org/10.1016/j.jmb.2015.01.013
Edited by A. Keating

Abstract

Despite the abundance of membrane-associated enzymes, the mechanism by which membrane binding stabilizes these enzymes and stimulates their catalysis remains largely unknown. Serum paraoxonase-1 (PON1) is a lipophilic lactonase whose stability and enzymatic activity are dramatically stimulated when associated with high-density lipoprotein (HDL) particles. Our mutational and structural analyses, combined with empirical valence bond simulations, reveal a network of hydrogen bonds that connect HDL binding residues with Asn168—a key catalytic residue residing >15 Å from the HDL contacting interface. This network ensures precise alignment of N168, which, in turn, ligates PON1's catalytic calcium and aligns the lactone substrate for catalysis. HDL binding restrains the overall motion of the active site and particularly of N168, thus reducing the catalytic activation energy barrier. We demonstrate herein that disturbance of this network, even at its most far-reaching periphery, undermines PON1's activity. Membrane binding thus immobilizes long-range interactions *via* second- and third-shell residues that reduce the active site's floppiness and pre-organize the catalytic residues. Although this network is critical for efficient catalysis, as demonstrated here, unraveling these long-rage interaction networks is challenging, let alone their implementation in artificial enzyme design.

Introduction

Popularly known as the "good cholesterol", serum high-density lipoprotein (HDL) particles play a key role in cholesterol transport and other anti-arteriosclerotic functions [1,2]. Apart from the scaffolding apolipoproteins and primarily apolipoprotein A-I (ApoA-I), different enzymes that play a role in lipid and cholesterol metabolism are known to attach to the membrane-like surface of HDL [3]. Among these is PON1—a human, calcium-dependent lipolactonase that also promiscuously catalyzes the hydrolysis of the organophosphate pesticide paraoxon. PON1 binds selectively to HDL particles, particularly those containing ApoA-I [4,5]. PON1's structural integrity and catalytic activity are utterly dependent on the presence of detergents and/or lipids. However, binding to HDL has a marked, selective effect on PON1's stability (the rate of inactivation due to calcium loss and misfolding decreases >350-fold) and its catalytic efficiency (k_{cat}/K_M) with lipophilic lactones increases by up to 20-fold relative to the detergent-associated enzyme [5,6]. The activity of the detergent-free enzyme is likely to be very low yet is impossible to determine because extensive delipidation results in complete loss of activity. Binding to HDL and the resulting catalytic stimulation also relate to PON1's anti-arteriosclerotic activity. Among other indications [7,8] are the differences associated with the 192Q/R human polymorphs. The 192Q isozyme binds HDL with lower affinity than the R isozyme and consequently exhibits reduced stability and lipolactonase activity [9].

The molecular details of PON1's HDL binding and catalytic stimulation are unknown. Indeed, although

membrane-associated enzymes are common [10], as is interfacial activation (namely, the stimulation of enzymatic activity upon membrane binding), its molecular basis is known for only a few enzymes [11,12]. PON1 is a six-blade β-propeller with a central tunnel containing two calcium ions. The tunnel buried calcium is critical for the enzyme's configuration stability, and the solvent-exposed calcium residing at the bottom of the active-site cavity is catalytic. Decorating the β-propeller scaffold are three helices that reside at the top of the active site. Two of these helices, H1 and H2, were suggested to play a role in PON1's anchoring to HDL [13] (Fig. 1a). Helix H1 serves as a membrane-anchoring helix, and its truncation reduces the affinity to HDL by ~100-fold. However, the

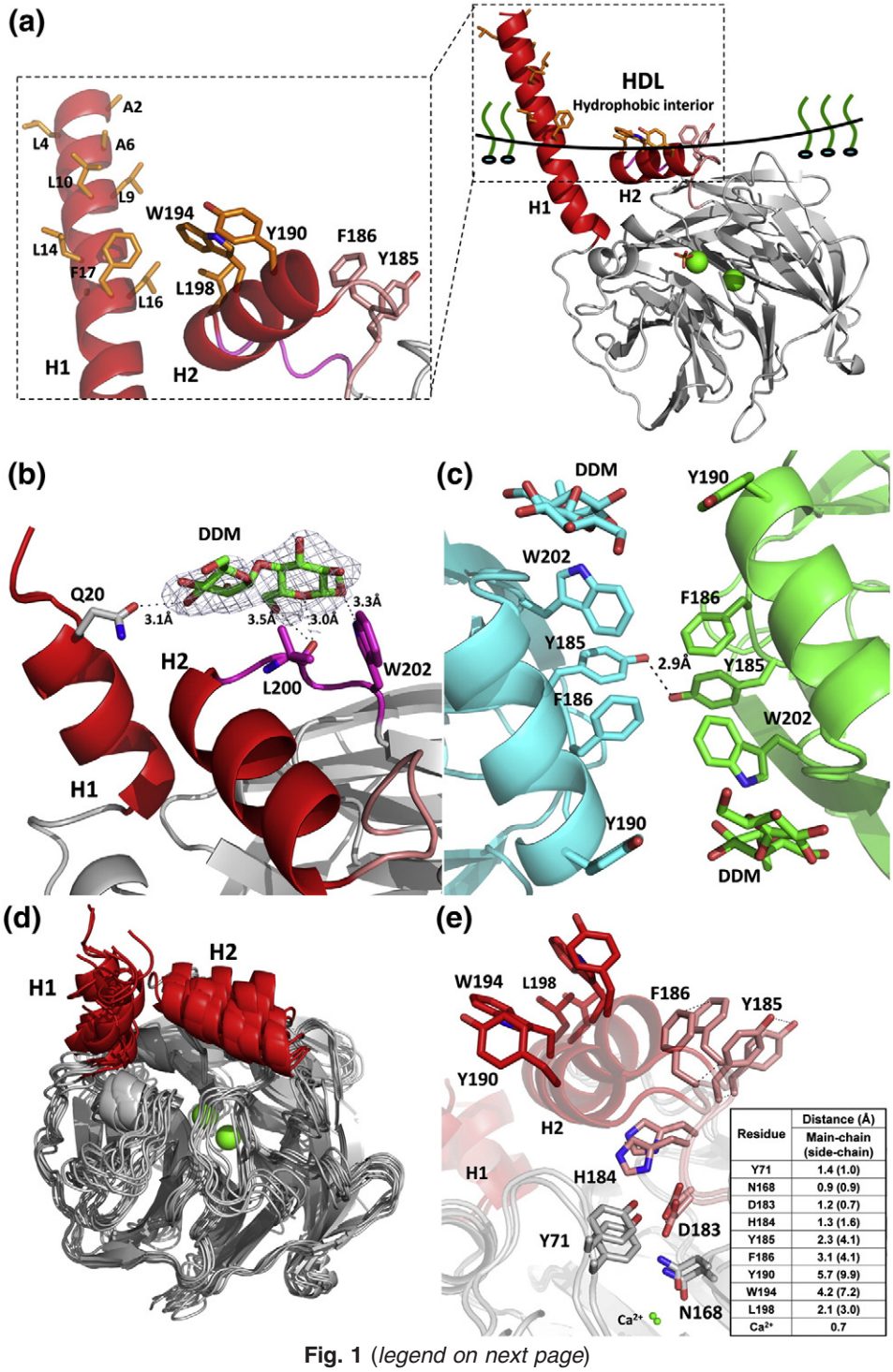

Residue	Distance (Å) Main-chain (side-chain)
Y71	1.4 (1.0)
N168	0.9 (0.9)
D183	1.2 (0.7)
H184	1.3 (1.6)
Y185	2.3 (4.1)
F186	3.1 (4.1)
Y190	5.7 (9.9)
W194	4.2 (7.2)
L198	2.1 (3.0)
Ca^{2+}	0.7

Fig. 1 (*legend on next page*)

H1-truncated enzyme retains relatively high affinity ($<10^{-7}$ M), presumably owing to interactions of H2 with HDL [5]. Direct evidence for H2's role is missing, however, and which of its residues mediate HDL binding is obviously unknown. Also unknown is the mechanism by which HDL binding stimulates the lactonase activity and why PON1's promiscuous paraoxonase activity is not stimulated. The selective stimulatory effect is particularly interesting because the postulated HDL binding interface resides at the periphery of the active site, ~20 Å away from the catalytic calcium at the bottom of the cavity.

Here, we describe mutational and structural analyses of PON1, along with computational simulations of its catalytic mechanism using different conformations that model the potential effect of PON1's interaction with HDL. We provide a detailed model for the binding of PON1 to HDL, specifically with respect to H2 residues, and of the mechanism of catalytic stimulation at an atomic level. We discuss implications of this model with respect to the role of membrane binding in interfacially activated enzymes. Finally, we underline more general implications regarding the importance of structural rigidity and the key role of second- and third-shell residues in configuring enzyme active sites. Specifically, comparison to other membrane-associated enzymes suggests that immobilization of the catalytic residues is a common feature of interfacial activation. Indeed, our results suggest that restraining unnecessary conformational freedom *via* second- and third-shell interactions comprises a general feature of enzyme catalysis.

Results

The PON1–HDL structural model

We have previously postulated the role of helices H1 and H2 in HDL binding based on the presence of exposed surface hydrophobic residues and especially of aromatic residues [5,13] (Fig. 1a). Our current analysis of crystal structures of PON1 in the region of helices H1 and H2 revealed potential interactions with a detergent molecule, *n*-dodecyl-β-D-maltoside (DDM), included in the crystallization medium. The detergent seems to interact with residues of H1 (e.g., Q20) and with the adjacent H2's C-terminal connecting loop (L200 and W202; Fig. 1b). Additionally, the packing surfaces between PON1 molecules within the different asymmetric units of the crystal's unit cell involve close interactions between the adjacent H2 helices and their connecting loops and specifically between Y185 and F186 of neighboring PON1 molecules (Fig. 1c). It appears therefore that the bound detergent molecules and the crystal packing interactions involving H1 and H2 play a major role in limiting PON1's conformational flexibility thereby prompting crystal formation.

Given the hydrophobic nature of these interactions, they are likely to mimic PON1's binding interactions with HDL. However, the H1 and H2 configuration seen in the crystal structure represents only one out of many possible configurations available for these helices. As conformational flexibility promotes faster unfolding rates and thereby lower stability [14–16], HDL binding increases the enzyme's thermodynamic stability as does detergent binding, though to a lesser extent. Similarly, the immobilization of a specific active-site configuration may account for the HDL-induced increase in catalytic efficiency.

Our working hypothesis has therefore been that HDL binding immobilizes the bound PON1 parts and, in turn, affects the active site's shape and catalytic organization. Indeed, the *B*-factors of PON1 structures indicate that the C-terminal end of H1 (the N-terminus is completely disordered) and H2 comprise PON1's most mobile parts (Fig. S1). Accordingly, the normal mode analysis of these structures revealed that helices H1 and H2 show large coordinated motions. This motion seems to infiltrate into the active site and affect the position of catalytic residues, foremost of N168 (a calcium-ligating residue) and the catalytic calcium (Fig. 1d and e).

Fig. 1. Structural features of H1 and H2. The analysis was based on the PON1 ligand-free structure, PDB code 3SRE. (a) The proposed model for anchoring of PON1 to HDL. This model suggests the interactions of PON1's helices (highlighted in red) H1 and H2 with the HDL's surface. Hydrophobic residues that reside on helices H1 and H2 and on H2's N-terminal connecting loop that are proposed to mediate HDL anchoring are shown in orange and salmon, respectively. A close view to the proposed PON1's interaction surface with HDL is also shown (H2's N-terminal and C-terminal connecting loops are highlighted in salmon and magenta, respectively; H1's residues 1–20 were modeled since their electron density in the crystal structure could not be defined). (b) A view of the interactions of the observed part of a detergent molecule, DDM molecule (green; shown is the sugar moiety and electron density for the lipophilic chain of DDM could not be defined; the $F_o - F_c$ omit map is contoured at 3σ). Shown are the contacting residues of H1 (gray) and of H2's C-terminal connecting loop (magenta). (c) View of the crystal packing interactions within different PON1 molecules (green and cyan) within unit cells of PON1's crystal structure. The contacts include the H2 helices and their N-terminal connecting loops. (d) Superposition of the normal modes, as predicted by elNémo, indicates the high mobility of helices H1 and H2 (in red). (e) PON1's two edge normal mode configurations. Shown are key H2 residues (Y190, W194 and L198) and of its N-terminal connecting loop (Y185 and F186), and the adjacent active-site residues (the D83–H184 dyad, the active-site mobile loop's residue Y71 and N168 that ligates the catalytic calcium; green sphere). The inset lists the displacement distances of main (C^α atoms) and side chains between these two edge configurations (most distant atoms).

We subsequently sought to experimentally explore the role of H2 residues in HDL binding and enzymatic stimulation. To this end, we also established a new experimental protocol.

In situ, cell-free expression of PON1 with reconstituted HDL

The traditional protocol applied for the analysis of PON1's interaction with HDL includes (i) production of recombinant PON1 or serum purification to obtain human PON1 in the presence of a detergent, (ii) delipidation to remove the detergent and (iii) incubation of detergent-depleted PON1 with HDL [3,5,17]. Aside from being laborious, this protocol is problematic due to the rapid inactivation of the dilapidated PON1. Thus, the observed stimulation might be over-estimated when normalized to a control sample with no lipids. To enable faster and more reliable analysis, we applied the cell-free *in situ* expression of recombinant PON1 in the presence of reconstituted, ApoA-I-based HDL particles (rHDL) [6,17]. We validated the reliability of this procedure by testing the activity stimulation with a chromogenic lactone substrate, TBBL, and with paraoxon. We measured the activity of cell-free expressed PON1 in the presence of rHDL at 0–10 μM concentration (Fig. 2).

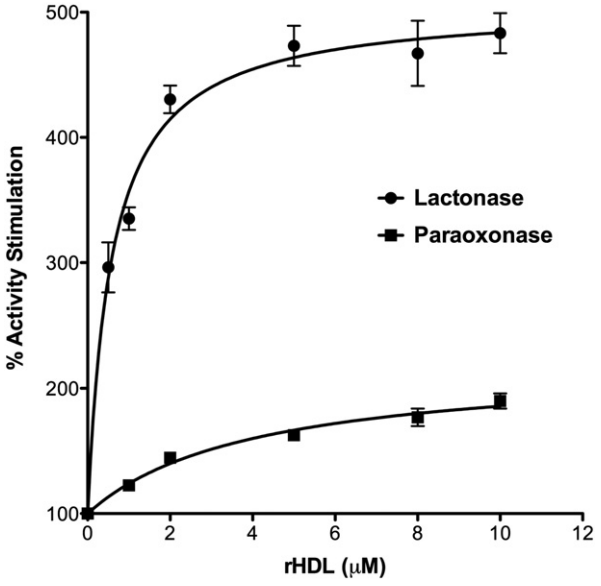

Fig. 2. A typical activity stimulation plot obtained with *in situ* expression of recombinant PON1 in the presence of reconstituted HDL particles. Enzymatic activity was tested with TBBL (0.25 mM) and paraoxon (1 mM). Stimulated activity is presented as the percentage of the initial activity of the *in situ* produced enzyme in the absence of rHDL. Standard errors for repeated experiments were ≤10% of the obtained stimulation factors.

The results obtained with this new procedure were in agreement with the previously applied delipidation protocol [5,6]. In essence, PON1's lactonase activity was stimulated by HDL following a typical Langmuir isotherm. The v_{max} (percent of activity relative to the activity of cell-free translated PON1 with no rHDL) and K_{app} (rHDL concentration that gives 50% of the activity stimulation) values were similar to those obtained with the concomitantly tested traditional protocol [K_{app} (μM) 0.58 *versus* 0.75 and v_{max} (%) 406 *versus* 414, respectively; Fig. S2a]. As previously observed [5], the paraoxonase activity was barely stimulated (Fig. 2), and no stimulation was observed with the H1-truncated PON1 mutant (Table 1).

The effect of rHDL on the stability of PON1 was explored using a previously applied inactivation assay [5,6]. The cell-free expressed PON1 samples with no HDL and at saturating rHDL concentration (10 μM) were incubated at 37 °C in the presence of a calcium chelator, ethylenediaminetetraacetic acid (EDTA). The residual lactonase activity was tested after 72 h and compared to the activity prior to EDTA addition (Table 1). The decreased inactivation rates upon HDL binding [5,6] were similarly reproduced (Table 1 and Fig. S2b). Moreover, as can be seen in Table 1, the lactonase stimulation and the stabilization effect are largely correlated.

Mutational analysis of H2 and its N-terminal loop

Truncation of H1 results in an ~100-fold drop in HDL affinity and no HDL-mediated stabilization and enzymatic stimulation, thus providing evidence for the role of the H1 helix in the HDL binding [5] (Table 1). Since truncation of H2 is not an option, point mutations were instead explored.

H2 and its N-terminal loop possess a stretch of hydrophobic surface side chains including Y190, W194 and L198, as well as the N-terminal loop residues Y185 and F186 (Fig. 1a). These positions are highly conserved in mammalian PON1s [18]—a degree of conservation that is atypical for surface residues. Some positions are fully conserved (e.g., positions 183–186) and others show only conservative substitutions (e.g., position 190, Tyr *versus* Phe). We designed mutants that sample residues Y190, W194 and L198, as well as Y185 and F186 within H2's N-terminal loop (Fig. 1a). Single substitutions to Ala of the H2 residues (i.e., Y190, W194 and L198) resulted in a relatively mild decrease of the HDL-induced stabilization and lactonase stimulation (Table 1) likely because of the existence of an entire cluster of hydrophobic residues on H2 (Fig. 1a). The 190–194 double mutant, however, showed almost no stimulation or stabilization (v_{max}/K_{app} values reduced by ~14-fold).

Mutations in H2's N-terminal loop also exhibited a marked effect. While Y185A showed comparable parameters to that of the wild type, Y185G, which presumably introduced changes not only in the side

Table 1. Activity stimulation and inactivation rates of PON1 and its mutants

Variant	Activity stimulation[a]			Inactivation[b]
	K_{app} (μM)[c]	v_{max} (%)[d]	v_{max}/K_{app} (μM^{-1})	Residual lactonase activity (%)[e]
PON1	0.58 ± 0.07 (1)	406 ± 11 (1)	700 ± 86 (1)	80 ± 7 (1)
Δ20-PON1	>10[f] (> ↓17)	—	—	20 ± 6 (↓4)
Y185A	0.68 ± 0.1 (↓1.2)	484 ± 19 (↑1.2)	712 ± 105 (1)	71 ± 4 (↓1.1)
F186A	2.4 ± 0.3 (↓4)	331 ± 15 (↓1.2)	138 ± 18 (↓5)	11 ± 1 (↓7)
Y185A/F186A	2.9 ± 0.7 (↓5)	183 ± 17 (↓2.2)	63 ± 16 (↓11)	6 ± 2 (↓13)
Y185G	>10[f] (> ↓17)	—	—	15 ± 3 (↓5)
F186G	1.5 ± 0.4 (↓2.6)	159 ± 13 (↓2.6)	106 ± 30 (↓6.6)	7 ± 1 (↓11)
Y190A	1.3 ± 0.3 (↓2.2)	268 ± 17 (↓1.5)	206 ± 49 (↓3.4)	59 ± 2 (↓1.4)
W194A	0.46 ± 0.13 (↑1.3)	188 ± 10 (↓2.2)	409 ± 118 (↓1.7)	73 ± 5 (↓1.1)
Y190A/W194A	3 ± 1 (↓5.2)	152 ± 18 (↓2.7)	51 ± 18 (↓13.7)	36 ± 1 (↓2.2)
L198A	2.2 ± 0.2 (↓3.8)	518 ± 19 (↑1.3)	259 ± 23 (↓2.7)	47 ± 6 (↓1.7)
Y71F	0.8 ± 0.1 (↓1.4)	467 ± 14 (↑1.2)	584 ± 75 (↓1.2)	75 ± 5 (↓1.1)
Y71G	1.70 ± 0.09 (↓2.9)	430 ± 7 (↑1.1)	253 ± 14 (↓2.8)	73 ± 6 (↓1.1)
H184Q	1.5 ± 0.2 (↓2.6)	367 ± 12 (↓1.1)	245 ± 34 (↓2.9)	34 ± 3 (↓2.4)
H184T	1.00 ± 0.09 (↓1.7)	613 ± 14 (↑1.5)	613 ± 57 (↓1.1)	96 ± 8 (↑1.2)

The TBBL concentrations used in the activity stimulation and inactivation are 0.25 mM and 0.5 mM, respectively.
[a] Stimulation of PON1's lactonase activity of PON1 by rHDL (determined at 0–10 μM rHDL; see Materials and Methods).
[b] Inactivation of PON1 by EDTA (15 mM).
[c] K_{app} is the concentration of rHDL that gave half-maximal stimulation of activity.
[d] v_{max} values are presented as the percentage of activity relative to re-PON1 expressed in the absence of rHDL.
[e] The residual lactonase activity is presented as the percentage at 72 h of incubation at 37 °C relative to time = 0.
[f] Reaction rates did not show saturation, and thus, an upper limit for the K_{app} value was provided based on the maximal rHDL concentration used. In brackets is the fold-decrease or fold-increase relative to wild-type PON1.

chain but also in the loop's backbone configuration, resulted in near-complete loss of the HDL effects. Both F186A and F186G resulted in a decrease in lactonase stimulation and stability, and the Y185A/F186A double mutant showed a near-complete loss of lactonase stimulation and stabilization (Table 1). Notably, in the absence of HDL, all these mutants exhibited rates similar to or even slightly higher than wild-type PON1, thus excluding the possibility of global effects on PON1's activity and stability (Table S1). Overall, these results support the hypothesis that residues of helix H2 and its connecting loop play a key role in PON1's binding to HDL and its catalytic stimulation.

The mechanism of PON1's catalytic stimulation

The long loop that extends from H2's N-terminus connects to PON1's scaffold and active site (Figs. 1a and 3). This loop also includes two residues, H184 and D183, which are part of the active-site wall. Mutations in these two residues have a drastic effect on PON1's activity [19–21]. However, neither of these residues is involved in catalysis, for example, as a base or an acid catalyst [21], nor is in direct contact with the lactone substrate [22]. Nonetheless, these residues and especially D183 are highly conserved, including in bacterial PONs that exhibit <30% sequence similarity to mammalian PONs [18]. What then is the role of H184 and D183?

A network of hydrogen bonds extends from H2's C-terminal loop *via* residues H184 and D183 to two active-site residues that are in direct contact with the substrate: Y71 at the tip of a highly mobile active-site loop (residues 70–81; Fig. 3, in light blue) and N168 that ligates the catalytic calcium (green sphere). Conformational variations in the mobile active-site loop, as well as in the catalytic calcium, modulate

PON1's catalytic activity and specifically relate to the enzyme's dual activity as a lactonase (the native activity) and as a paraoxonase (a promiscuous activity) [22,23]. We thus reasoned that the lactonase stimulation upon HDL binding might be mediated *via* this network and the contacts to either Y71 or N168 (Fig. 3).

To examine these two options, we prepared a set of mutants in residues that are part of the network that includes D183, H184, Y71 and N168 (Fig. 3). As previously reported, mutations in positions 183 and 168 resulted in a drastic decrease of both lactonase and paraoxonase activities [20,21,23]. Mutants that did exhibit detectable activity included Y71F, Y71G, H184Q and H184T. Since these mutations had a relatively mild effect on the lactonase activity (Table S2 and Ref. [21]), we could specifically test for HDL stimulation effects. The conservative mutation Y71F that abolishes the putative hydrogen bond between Y71's hydroxyl group and even the drastic Y71G mutation resulted in only a mild decrease in the HDL-induced stabilization and catalytic stimulation (<3-fold; Table 1). This combined with simulations (described below) indicating that Y71 shows only minor displacements in response to changes in H2's repositioning suggest that Y71 does not play a key role in PON1's lactonase activity in general and in the HDL-induced stimulation specifically.

The hydrogen bonds spanning from H2, including K192, to N168 are much more likely to modulate catalysis. This hypothesis is supported by N168 being intolerant to replacements (mutants of the other calcium-ligating residues, 53, 224, 269 and 270, show some residual activity [23]), by the immutability of D183 despite having no direct role in catalysis [21] and by the effects of the 192Q/R polymorphism on HDL binding and stimulation [9,24]. The role of H184 in aligning D183 and, in turn, N168 is supported by the fact that mutations of H184 to non-polar residues (e.g., to Ala) result in a drastic reduction of PON1's activities [19–21]. However, hydrogen bond donor residues such as glutamine or threonine retained the lactonase activity and stimulation or even slightly increased the HDL stimulatory effect (H184T; Table 1). Further, PON1's denaturation is initiated by the loss of the catalytic calcium, followed by loss of the structural one and irreversible unfolding [5,25]. The spatial fixation of N168 by the D183–H184 dyad and the accompanying electrostatic effects that stabilize the catalytic calcium ion (see computation results below) are likely to have a significant contribution to PON1's affinity to the catalytic calcium. Thus, limiting the conformational freedom at the H1–H2 interface (Fig. 1d and e) and thereby reinforcing the hydrogen bond network that immobilizes N168 and in turn the catalytic calcium (Fig. 3) is the most likely explanation for the effects of HDL binding on PON1's lactonase activity and configurational stability.

Empirical valence bond simulations

A crystal structure of PON1 (or any enzyme for that matter) bound to HDL is unavailable. Thus, to better understand the structural changes induced by HDL binding and to unravel their effect on the active site's configuration, we performed empirical valence bond (EVB) simulations [26] using PON1's crystal structure (PDB code 3SRG) and a set of snapshots borrowed from the structure's most representative normal modes. Our working assumption has been that the changes in PON1's lactonase activity upon HDL binding relate primarily to H2's conformation as indicated by the abovementioned data. The simulations were performed in the presence of a lactone substrate, TBBL, that represents PON1's lipophilic lactone substrates, and with paraoxon, a promiscuous substrate. With each substrate, six different PON1 conformations were considered in order to explore the relationship between H2 conformation and catalysis. These included the original crystal structure and snapshots of the largest displacements of the H1 and H2 helices along the five most representative normal modes of the enzyme (Fig. 1d). The H2 displacement observed within these normal modes was 4.9 Å (maximal RMSD for all H2 C^{α} atoms within the six structural models). H1 is overall more flexible and its membrane-embedded N-terminus was not included in the structure and models; however, the displacement of its C-terminal part that connects to H2 and to PON1's active site is in the range 5 Å (RMSD for C^{α} of residues 20–31). The remaining parts of PON1 are obviously far more rigid (maximal RMSD for all C^{α} atoms except H1 and H2 is 1.5 Å). While none of these conformations is necessarily identical with the actual conformation of PON1 when associated with HDL, they provide a plausible set of starting conformations for the simulations and thus allowed us to directly probe how changes in H2's position affect the calculated energetics.

For simulating the lactonase activity, our models for both the crystal structure and the snapshots from the different normal modes were based on H115 as the general base generating the hydroxide nucleophile [22]. The nucleophile attacks from a non-inline position to form a tetrahedral intermediate with an elongated C–O bond to the ring oxygen, which then breaks to open the ring (Figs. S3 and S4). However, we note that, in the refined active-site model presented here, the lactone ring oxygen points toward N224 rather than toward D269 as in the earlier model (see Figs. 6 and 9 in Ref. [22]). The free energies of activation for the rate-determining step (the nucleophilic hydroxide attack to form a tetrahedral intermediate) for these models are shown in Table 2. For computational simplicity, only the rate-determining step was considered in this case thus allowing for greater simulation time for the different PON1 conformations considered.

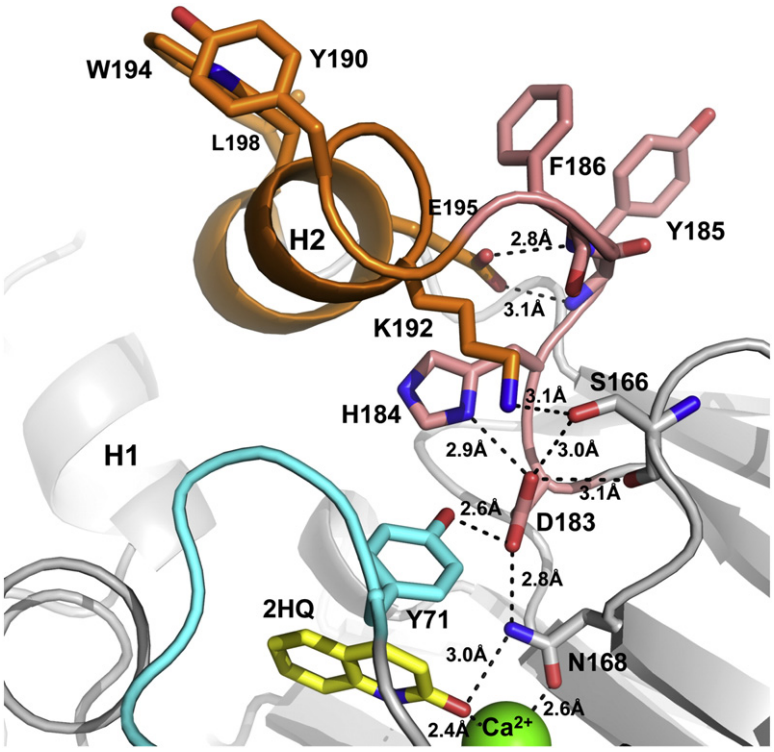

Fig. 3. H2's N-terminal connecting loop and its interactions with the PON1's catalytic machinery (PDB code 3SRG). Shown is the lactone analogue 2-hydroxyquinoline (2HQ, in yellow) and Y71 that resides in an active-site mobile loop (cyan). Broken lines represent putative hydrogen bonds of D183 and H184 to H2 residues (orange) to H2's N-terminal loop (salmon) and to the catalytic calcium-ligating residue N168 (gray). Our model suggests that HDL binding results in the fixation of H2 and its N-terminal loop. Immobilization of these floppy parts of the enzyme (Fig. 1d and e) results in spatial fixation of the D183–H184 dyad and, in turn, of N168 and the catalytic calcium, thus accounting for the dramatic increase in PON1's stability and the stimulation of its lactonase activity.

The data indicate that the calculated activation barrier varies significantly with the positioning of H2 despite residues from this helix having no direct contact with the substrate. Also computed were the distances between the catalytic Ca^{2+} ion and the oxygen atoms of its ligating residues (using the central atom of the dummy model; see Materials and Methods and Supplementary Information). Indeed, the largest and most consistent displacements of the ligating residues are seen with N168, in both lactone and paraoxon models (Table S3).

HDL binding restrains the floppiness of PON1's active site

In our simulations, both N168 and Y71 are quite floppy and reposition according to the substrate's position. Y71 appears to reposition in order to make space for the lactone's tail (repositioning is more pronounced in the case of paraoxon [22], as also discussed below). Similarly, there appears to be a "tug-of-war" between the lactone's carbonyl oxygen and N168 and N224 for chelation to the catalytic Ca^{2+} ion, with some TBBL positions displacing these residues from the metal (Fig. S4). Indeed, N168 *a priori* forms a relatively weak interaction with the catalytic metal—2.6 Å O–Ca distance *versus* ~2.2 Å for N224 and N270 that also ligate the catalytic calcium (typical M–O distances for Ca^{2+} are in the range 2.4 Å; see Ref. [27]). Furthermore, the H2 configuration that results with N168 conformations with the tightest initial metal coordination distances are also those that give the lowest activation barriers and hence the highest catalytic efficiencies (NM10 with TBBL and NM7 with paraoxon; Table 2 and Table S3).

The key critical interactions, however, are seen upon the development of the transition state and ultimately the tetrahedral intermediate (Fig. S4d). Specifically, the formation of the tetrahedral intermediate involves the displacement of significant charge density onto the metal-ligating carbonyl oxygen atom of the lactone substrate, as indicated by the calculated partial charge differences between the resting state and the intermediate (partial charges provided in Supplementary Information) and as are the electrostatic contributions of individual residues to transition state and intermediate stabilization for different key PON1 conformations (Fig. S5). In the lactonase simulations exhibiting the lowest activation energies, N168 and, most importantly, H115 are optimally aligned to stabilize the newly developing negative charge, resulting in a barrier reduction of ~8 kcal/mol compared to the background reaction and a stabilization of 10 kcal/mol of the tetrahedral intermediate. Upon perturbing H2's position, as simulated by the different normal modes, the increase in the calculated activation barrier directly correlates with decreases in the enzyme's ability to stabilize the tetrahedral intermediate. Thus, the observed changes in the activation barrier are pure Hammond effects, namely, changes in the electrostatic pre-organization of the active site and thereby in its ability to stabilize the intermediate and enhance the

Table 2. Calculated activation and reaction free energies for PON1's lactonase (TBBL) and paraoxonase activities using different starting conformations of the enzyme

System[a]	$\Delta g^{\ddagger}$[b]	ΔG_0[b]	$\Delta\Delta g^{\ddagger}$[b]	H2, initial[c]	H2, after 5 ns[c]
Lactonase activity					
NM10	12.2 ± 0.8	3.8 ± 1.4	−2.0	4.36	4.58 ± 0.18
NM11	14.0 ± 1.1	6.7 ± 1.5	−0.2	1.09	1.78 ± 0.15
Crystal structure	14.2 ± 0.7	8.8 ± 1.3	0.0	0.00	1.48 ± 0.14
NM9	16.4 ± 0.4	11.6 ± 0.6	+2.2	1.15	1.98 ± 0.23
NM8	17.8 ± 2.1	11.2 ± 2.0	+3.6	2.39	2.73 ± 0.09
NM7	18.1 ± 0.5	13.7 ± 0.8	+3.9	1.76	2.96 ± 0.29
Paraoxonase activity					
NM7	14.9 ± 0.5	−11.8 ± 1.0	−1.8	1.76	2.87 ± 0.25
NM8	16.7 ± 0.6	−8.7 ± 1.7	0.0	2.39	2.80 ± 0.16
Crystal structure	16.7 ± 0.7	−7.2 ± 1.0	0.0	0.00	2.14 ± 0.60
NM9	17.4 ± 06	−10.4 ± 1.6	+0.7	1.15	1.73 ± 0.13
NM10	22.1 ± 0.7	−1.2 ± 0.9	+4.7	4.36	4.38 ± 0.25
NM11	26.0 ± 0.8	−5.6 ± 4.0	+11.1	1.09	1.69 ± 0.10

Shown here are also the RMSD values of the H2 helix in the different structures with respect to the initial crystal structure.
Energy values are averages and their standard deviations for 15 individual EVB simulations taken from snapshots along the MD equilibration for each of the relevant systems (i.e., a total of 150 individual EVB trajectories for the enzyme-catalyzed reactions and 30 EVB trajectories corresponding to the background reaction).

[a] NM7 to NM11 denote EVB simulations starting from snapshots along five different normal modes of PON1, as illustrated in Fig. 2 and discussed in the methodology section.

[b] $\Delta g^{\ddagger}$ and ΔG_0 denote the calculated activation and reaction free energies, respectively, as averages over 15 EVB simulations, and $\Delta\Delta g^{\ddagger}$ denotes the $\Delta g^{\ddagger}$ difference between the crystal structure and the structure from the respective normal mode. Note that "reaction free energy" denotes the calculated free energy for the transition from the enzyme-bound reactant to the enzyme-bound intermediate states, respectively. The corresponding experimental $\Delta g^{\ddagger}$ values for the enzyme catalyzed reaction for TBBL and paraoxon are 14.9 kcal/mol and 16.5 kcal/mol, respectively, based on enzymatic parameters presented in Table 1 and [23].

[c] "H2 initial" refers to the relevant structure (either the crystal structure or a snapshot from the normal mode analysis) before any MD equilibration, using the crystal structure as a frame of reference. "H2 after 5 ns" is the average RMSD over the initial 5 ns of equilibration for each system, collecting data ever picosecond (note that subsequent EVB calculations were cumulatively on the microsecond timescale). All energies are given in kilocalories per mole, and RMSD values are given in angstroms.

rate of lactone hydrolysis. Intermediate stabilization is also facilitated by slight relocation of N168, which in the most active model goes further away from the metal and more closely interacts with the developing negative charge on the carbonyl of the lactone substrate (NM10; Table 2). This relocation is dependent on a tight network of hydrogen bonds that positions N168 for optimal catalysis. Indeed, in the least reactive model (NM7), this network is broken making N168 too floppy for optimal catalysis. Accordingly, the restrained dynamics of PON1 upon association with lipids and detergents in general, and HDL specially, have a profound effect on this enzyme's ability to achieve and maintain this pre-organized catalytic conformation and its overall structure.

Lack of stimulation of the paraoxonase activity

Unlike PON1's lactonase activity, the promiscuous paraoxonase activity is largely unaffected by HDL binding (Fig. 2). To explain this difference, we examined EVB models of paraoxon hydrolysis [23] (Fig. S3). A summary of the structural and energy data are presented in Table 2 and Tables S3 and S4. In PON1's catalysis of paraoxon hydrolysis, the nucleophile optimally attacks from an inline position with the P–O bond to the *p*-nitrophenyl leaving group [28]. In fact, PON1 uses a different subset of residues to facilitate these two different reactions [22,23] and thus changes in the network connecting H2 to N168 may have different effects on these two reactions. As proposed before [23,29], the modeled nucleophile was a water molecule optimally positioned between D269 and E53 for direct inline attack of paraoxon. This mechanism was further validated by the simulations as, despite the weak restrains applied, the optimal substrate and transition-state binding modes observed in the simulations were in agreement with mechanism. Further, the crucial interaction of lactones with H115 was not observed in our simulations with paraoxon, in accordance with mutations of H115 being neutral or even beneficial to PON1's paraoxonase activity [23]. Accordingly, in all our stimulations, protonation of D269's side chain results in dissociation of this residue from the catalytic Ca^{2+} ion and substantial metal displacement toward H115 and N168—such displacements have also been observed experimentally [23]. Moreover, as with the lactonase simulations, the structure with the lowest activation barrier (NM7) is also the structure with the most stable metal coordination, particularly with respect to N224 and D269. Finally, paraoxon is an "opportunistic" substrate and also takes advantage of the displacement of the flexible loop containing Y71 to create a

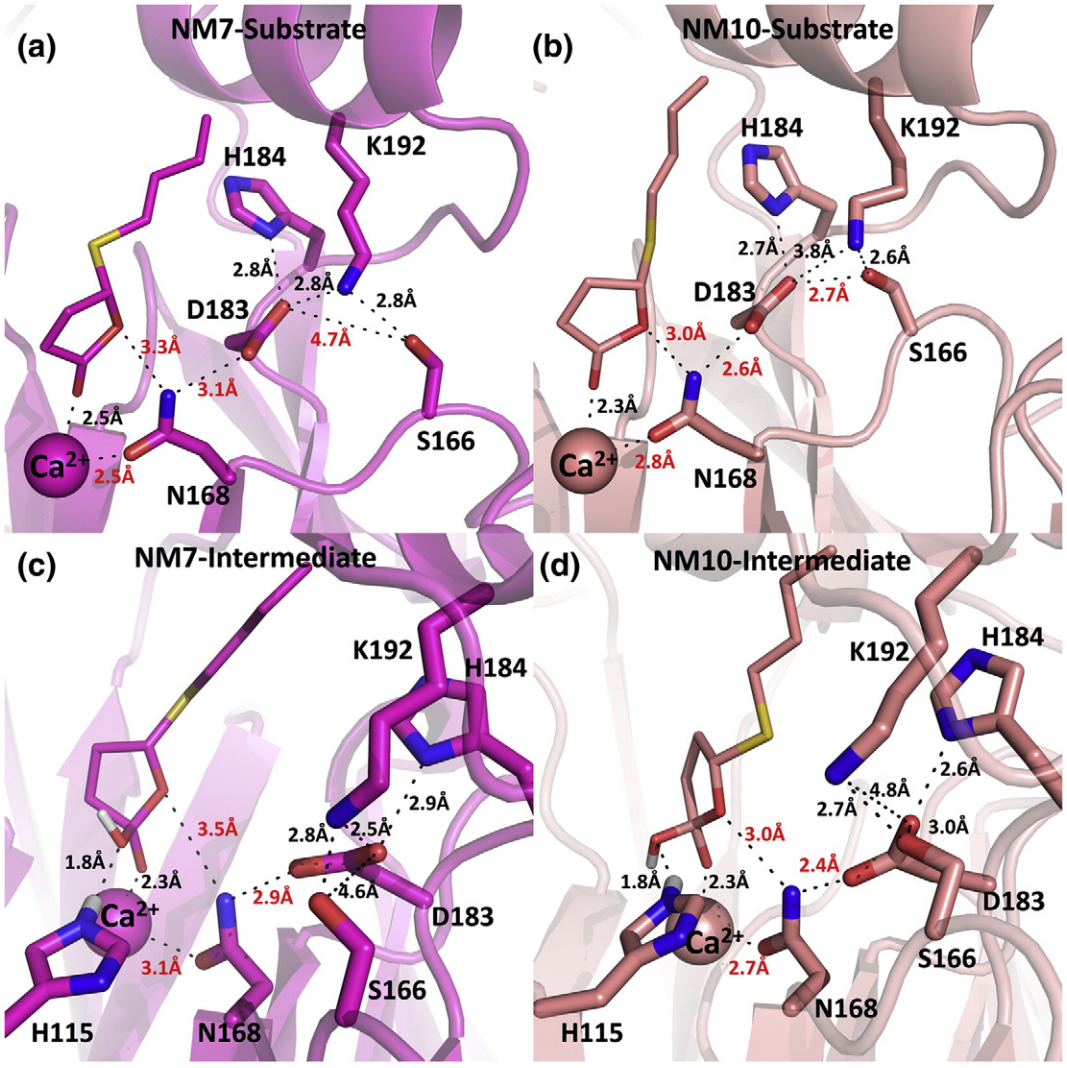

Fig. 4. The effect of H2 adjustment on the active-site architecture and substrate catalysis. Shown are NM7 (the least reactive configuration; magenta) and NM10 (the most reactive configuration; salmon) after 5 ns MD equilibration with the lactone substrate (a and b) and with corresponding intermediate state after EVB simulations (c and d). The distances between key residues connecting N168 to the H2 helix through K192 are indicated, as well as the N168–Ca^{2+} interactions (key interaction changes are highlighted in red). Note that NM7 and NM10 are the structures that give the highest and the lowest lactonase activation barriers, respectively (Table 2).

binding pocket large enough to accommodate this bulky substrate [22,23]. This is also indicated by mutations to hydrophobic residues such as Y71F having a small effect (~6-fold reduction in the paraoxonase activity) as compared to ~120-fold reduction in Y71G (unpublished data) (see also Fig. S6a).

Overall, the experimental data and EVB simulations coincide in indicating that the promiscuous paraoxonase activity is mediated by an active-site configuration that is fundamentally different from the one executing the native lactonase function and that these reaction proceeds through a different mechanism (D269 rather than H115 acting as a general base, with inline rather than non-line attack). Foremost, the simulations indicate that the most optimal mode for paraoxon, NM7, is the poorest one for the lactonase activity and the most active lactonase mode, NM10, is the next poorest one for the paraoxonase (Table 2).

Finally, note as a side observation that PON1 appears to keep the lactone substrate in a water-excluded hydrophobic cage with only two active-site water molecules retained in the simulated substrate and intermediate complexes (Fig. S6b). This substrate-binding configuration has the benefit of enhancing electrostatic effects in a low dielectric environment and thus in accelerated rates (discussed recently in Ref. [30]). It would not be unreasonable to assume that the water-exclusion effect is amplified

upon interaction with detergents, lipids let alone with HDL (in themselves acting as "plugs" to exclude solvent). In the case of the paraoxonase activity and its optimal active-site configuration (NM10), the water-exclusion effect is less pronounced with ~7 water molecules within 5 Å of the substrate at the reactant state, ~3 water molecules at the transition state (all interacting with the nitro group of the phenoxy leaving group) and 5 water molecules at the product state (not including the nucleophile and a metal-coordinating water molecule and based on examining a representative NM10 EVB trajectory).

The interaction network aligning N168 and the catalytic calcium

A closer examination of the average distances over the course of the EVB trajectories reveals that the most significant changes occur in the interaction patterns between H2 residue K192, *via* S166 and D183, down to N168 and the catalytic calcium (Fig. 4). Specifically, in NM7, the least reactive configuration, K192, is displaced and becomes positioned between S166 and D183 (Fig. 4a). The N168–Ca^{2+} interaction is consequently weakened and the activation barrier increases by 6 kcal/mol compared to the most reactive conformation (Fig. 4a and c, Table 2 and Table S3). In contrast, in NM10, the most reactive configuration, the interaction network results in N168 being optimally positioned to stabilize the intermediate's developing negative charge (Fig. 4c and d and Fig. S5). The potential importance of S166 has also been observed in molecular dynamics (MD) simulations of PON1 [29]. It therefore follows that HDL binding stabilizes a particular conformation of H2 and of H2's residues that face the active site, thereby reducing the representation of alternative active-site configurations whereby N168 and the catalytic calcium are misaligned.

In addition to direct effects on PON1's catalytic center, a secondary effect of HDL association appears to be a better fit of the binding pocket for the alkyl tail of the lactone substrate. Specifically, in the original crystal structure, there is a potential steric clash between the alkyl tail of the modeled lactone substrate and M196's side chain (as well as, in some simulated structures, of K192's) (Fig. S7). In our most reactive models, H2 is slightly displaced inward and sideways, and both K192 and M196's side chains are shifted to enable higher complementarity with the bound lactone. Therefore, a secondary effect of HDL association might be tighter substrate binding. Indeed, lactones with longer alkyl chains display higher HDL stimulation factors [5].

Interestingly, in the case of the paraoxonase activity, the effects of K192's displacement is manifested in the electrostatic contributions of individual protein residues to transition state and/or intermediate stabilization in the most and the least reactive configurations for lactone and paraoxon hydrolysis, respectively (Fig. S5). For lactone hydrolysis, there are large stabilizing contributions from H115, N168 and K192 in the most reactive conformation (NM10), and these are all substantially diminished in NM7, the least reactive conformation. In contrast, the only significant change in individual residue contributions to paraoxon hydrolysis comes from K192 whose contribution is diminished in NM11 (the least reactive configuration). In the latter, the K192-S166-D183-N168 interaction network is disrupted, as indicated by this configuration having a suboptimal activation barrier for lactone hydrolysis, but the positively charged lysine is placed closer to the lactone's anionic leaving group, thus resulting in an overall favorable activation barrier energy. Thus, as described above, the same enzyme conformation can have orthogonal effects on the two different activities.

The role of K192 in the HDL-mediated stimulation is also indicated by the effects of the human PON1 192R/Q polymorphs. Both *in vitro* and *in vivo*, the 192Q isozyme exhibits significantly lower HDL binding and lactonase stimulation than 192R. Recombinant PON1 exhibits >91% sequence identity to rabbit PON1 and, accordingly, has Lys at position 192. Recombinant PON1-192K and PON1-192R show essentially the same level of stability and activation upon the association to HDL, whereas, similarly to the human isozyme, recombinant PON1-192Q shows reduced stability and stimulation [9]. The 2.3-Å crystal structure of re-PON1-192Q provided here (Table S5) indicated no major changes in backbone or side-chain orientations (Fig. S8a). However, the presumed hydrogen-bonding network that connects the H2 helix to N168 differs. The amide group of Q192 is in close contact with the backbone carbonyl of F186—2.9 Å *versus* 4.8 Å to the α-amino group of 192 K; the distance to the side chain of S166 is also shorter (2.6 Å *versus* 3.1 Å in 192 K; Fig. S8). F186 seems to be involved in HDL binding as indicated by the effects of the F186G mutation (Table 1). It is therefore likely that the K192Q mutation stabilizes an unfavorable configuration of H2's N-terminal connecting loop such that the HDL binding effects are markedly reduced. A similar yet more complex trend is observed in our simulations whereby the calculated $\Delta g^{\ddagger}$ values for the K192Q mutant fall in a much narrower range than for the wild-type enzyme, suggesting that this mutation exhibits reduced sensitivity to HDL binding (Table S4 and Fig. S8).

Discussion

We derived a detailed atomic model that indicates how the increased structural rigidity of PON1's active site that follows HDL binding (and detergent–lipid binding, to a lesser extent) and the precise alignment

of its key catalytic residues enhance the enzyme's catalytic efficiency. Our model is based on a large set of experimental data including crystal structures and mutants, as well as EVB simulations. The latter are crucial, as no structural method can unravel the structural features on the entire catalytic trajectory, let alone in the absence of structures of the PON1–HDL complex. We surmise, however, that, as specified in the next section, the tight correlation between the simulations and experimental results justifies the conclusions drawn here.

Reliability of the simulations

As discussed in the section Empirical valence bond simulations and in the supplementary information, one of the challenges of our computational model is the absence of HDL from our actual simulations. This limitation is a necessity due to the fact that there currently exists no available structure of PON1 (or in fact any other membrane-associated enzyme) in complex with HDL. However, even if such a structure existed, performing EVB simulations to the extent presented in the present work is computationally intractable. Detergent molecules could have arguably been included in the simulations. However, we presume that the primary effect of both detergents and HDL is in maintaining PON1' structural integrity and specifically in maintaining its active-site configuration by restraining the motion of H1 and H2. As the timescales of our simulations are too short for unfolding of the protein and all residues further than 25 Å from the reaction's center were largely restrained to their crystallographic coordinates (see the supplementary information for details), we surmise that the simulations as performed provide relevant insights as to how various configurations of H1 and H2 affect PON1's activity. The applied set of H1 and H2 configurations is also realistic—using the actual crystal structure, we obtained calculated activation barriers of 14.2 and 16.7 kcal/mol for lactone (TBBL) and paraoxon hydrolysis, respectively (Table 2), in agreement with the corresponding experimental values of 14.9 and 16.5 kcal/mol, respectively [23].

In addition to quantitatively reproducing the activation barriers for the reactions catalyzed by wild-type PON1, we reproduced a number of key structural features that increase our confidence in the qualitative information our simulations provide. For example, as outlined above, in the case of lactone hydrolysis, we observed a potential clash between the lactone's alkyl tail and the side chains of K192 and M196. These clashes are mitigated in the most reactive configurations (Table 2 and Fig. S7). This result accounts for the experimental observation that lactones with longer alkyl chains display higher HDL stimulation factors [5], suggesting that the HDL-bound configuration of H2 provides a binding pocket more suitable for long-chain lactones.

Foremost, the simulations had to account for the opposing effects observed with PON1's native lactonase activity *versus* its promiscuous paraoxonase activity, thus restricting the space of tunable computational parameters. Notably, in agreement with the minor effect of HDL on paraoxon hydrolysis, models based on the original, unperturbed crystal structure already indicate substantial activation barrier reduction compared to the background hydrolysis of paraoxon in water. Thus, the most optimal H2 position (NM7) only provides an additional barrier reduction of ~2 kcal/mol relative to H2's configuration in the crystal structure (as compared to the reduction of 4 kcal/mol in NM10, the optimal H2 configuration for the lactonase activity). Further, the displacement of K192 that was detrimental to lactone hydrolysis (Fig. 4a and c) is actually beneficial to paraoxon hydrolysis as it brings a positive charge closer to the phenoxy leaving group. The latter is in agreement with the experimental observation of the 192R human isozyme showing several-fold higher paraoxonase activity than 192Q [9,31].

Thus, although our simulations cannot reproduce all the effects of PON1's association with HDL, we could examine key features of PON1's structural dynamics and mechanism of catalysis and obtain a reasonable model describing the effects of HDL binding on PON1's lactonase and paraoxonase activities. The key feature here appears to be the fact that TBBL and paraoxon hydrolysis proceed through two different mechanisms, using different subsets of active-site residues. The optimal structure for lactone hydrolysis appears to involve a spatially fixated N168, therefore tightly positioning the catalytic calcium and H115's side chain. Indeed, both N168 and H115 are critical to stabilization of the developing negative charge of the lactone's oxyanion intermediate (for a quantitative comparison of electrostatic contributions, see Fig. S5a and b). In contrast, paraoxon hydrolysis is dependent on a floppy calcium [23] and hence, as indicated by both the simulations and the mutational data, the contributions from N168 (a key to the calcium's ligation) and H115 are far smaller.

The mechanism of HDL stimulation

PON1's mechanism of catalytic stimulation involves a complex network of interactions that spans over 20 Å, from H2 and H2's N-terminal loop (residues 183–187) into the very core of PON1's active site—the catalytic calcium ion. This network includes two active-site residues D183 and H184 that are absolutely essential and conserved but whose role remained thus far unknown. Our results indicate that D183, with the assistance of H184, plays a key role in aligning N168. The latter ligates the catalytic calcium and plays a role in aligning the

substrate for catalysis. The computational simulations also indicate that as a result of the very different requirements for catalysis, the same structural configurations have opposite effects on the lactonase and paraoxonase activities. However, for both substrates, rigidification of the active site is critical for high catalytic efficiency, as the presence of lipids or detergents is a prerequisite for PON1's structural integrity and catalytic activity. In general, detergents and lipids induce a significantly lower activity stimulation of PON1 in comparison to HDL. Many detergents and lipids [5,6,32,33] were shown to stabilize PON1 and induce some activity stimulation. However, none induced the same level of stability and activity stimulation obtained with HDL, even not the same types and compositions of lipids found in HDL particles (i.e., in the absence of apolipoprotein [5]). This might be due to the major differences in binding affinity and the mode of binding by HDL [5]. Indeed, the crystal structures of PON1 reveals that, despite the presence of detergent molecules, only weak hydrogen bonds connect helices H1 and H2 (distance of >3.0 Å; Fig. 1b); consequently, H1 is largely disordered and H2 is highly mobile (Fig. S1). HDL contains an apolipoprotein in addition to lipids. Specifically, ApoA-I induces the highest binding affinity and activity stimulation [5,6]. Altogether, our current data indicate that PON1's catalytic activity is highly sensitive to the configuration of helices H1 and H2 that mediate lipid binding. It is therefore likely that the HDL-bound configuration of PON1 does not significantly differ from the detergent–lipid configurations yet is more tightly and rigidly defined.

This study also augments our limited knowledge of how lipid interactions modulate the structure, stability, catalytic efficiency and specificity of membrane-associated enzymes (interfacial activation). The best-studied interfacially activated enzymes are lipases and especially secreted phospholipase A2 (sPLA2) [34]. The latter shares several features with PON1, such as the proximity of the active site to the membrane interface and having a highly mobile active-site loop. Analogously to PON1, truncation of the N-terminal helix of sPLA2 [35] and even point mutations resulted in significant decrease of both stability and activity of PLA2 [36,37]. Also, in resemblance to PON1, the N-terminal helix of sPLA2s (residues 1–12) shows high mobility in the lipid-free form [12]. This configurational flexibility infiltrates to the active site and specifically to the catalytic residues H48 and D99 [12]. It was therefore postulated that the lipid-bound sPLA2s adopts a conformation that reinforces the hydrogen bonds between catalytic residues and thereby leads to efficient catalysis [38]. The revealed mechanism of PON1's interfacial activation is similar, albeit not in the atomic details (as sPLA2 and PON1 differ in their fold and active sites) but in the overall effect of reducing the enzyme's conformational ensemble and aligning the key catalytic residues. This allows the enzyme to achieve lower activation energies and higher rates. Indeed, this case study of PON1 at atomic detail reveals the manner by which membrane binding propagates along long distances *via* a complex network of hydrogen bonds and critical mediators such as D183-H184. Interfacial activation, however, is not limited to only protein–membrane interactions, as protein–protein interactions may play a similar role *via* long-range interaction networks that connect interface residues with the key catalytic residues [39].

Active-site floppiness—The general implications

Beyond the effects of interfacial activation, it appears that restraining active-site floppiness, i.e., reducing unnecessary degrees of freedom of key active-site residues, is a challenge for enzyme catalysis. That is, as is seen with the effect of H2 mobility on PON1's enzymatic activation energy, the coexistence of multiple enzyme substrates (e.g., of different residue rotamers and protonation states and/or backbone configurations) is counterproductive with respect to rate acceleration, namely, catalysis of the chemical step. Widening of the conformational ensemble may also account for the gradual loss of rate acceleration (k_{cat}/k_{uncat}) with increased temperature, a loss that seems to occur in all enzymes including thermophilic ones and occurs within the range of temperatures that the folded state is fully maintained [40]. Active-site floppiness also seems to underline designed enzymes, where the conformation of key active-site residues is not sufficiently defined [41–43]. In the course of the evolutionary optimization of computationally designed enzymes, such alternative configurations are minimized but not completely eliminated [42]. Indeed, what designed active sites seem to be lacking most are the networks of interactions that align catalytic residues such N168 and the catalytic calcium in PON1. These networks include an array of second-shell residues (e.g., D183-H184) and third-shell residues (K192, S166 and H2 residues; Figs. 3 and 4). The essentiality of this network is manifested in the fact that disturbance of even its most far-reaching periphery (the absence of HDL interactions or at a minimum of detergent stabilization) or disturbance of second-shell residues such as D183 leads to a complete loss of activity.

Materials and Methods

Wild-type like PON1 mutants and kinetics

As in earlier studies, we used recombinant variants of PON1 [44]: G3C9 was used for the HDL–PON1 interaction analysis (native N-terminal and C-terminal His tag), whereas G2E6 (N-terminal His and Trx tags) was used

for structure determination. For simplicity, these wild-type-like PON1 variants are referred to in the text as PON1. Expression and purification of the wild-type-like PON1 mutants were performed as previously described [5,22]. Mutants for both the G2E6 and G3C9 variants were generated by transfer PCR [45] and verified by DNA sequencing. Rates with 5-thiobutyl butyrolactone (TBBL; lactonase activity) were determined at substrate concentrations in a range from 0.3 × K_M up to (2–3) × K_M and k_{cat}, K_M and k_{cat}/K_M were obtained by fitting the data to the Michaelis–Menten model with PRISM (GraphPad Software). The pH 8.0 buffer used for enzyme kinetics contained 1 mM $CaCl_2$, 0.1% Tergitol NP10, 50 mM Tris and 150 mM NaCl. All data presented are the means of ≥2 independent experiments, and the error ranges represent the standard deviation from the mean.

Preparation of rHDL

Recombinant human ApoA-I (kindly provided by Prof. Michael Oda, Oakland Research Institute) was expressed in *Escherichia coli* and purified as previously described [5,46]. Briefly, cells were re-suspended in phosphate-buffered saline (supplemented with 1 mM 1,4-dithiothreitol) and lysed by sonication. Cleared lysates were supplemented with 3 M guanidine hydrochloride, purified to homogeneity on a Ni-NTA column and dialyzed against Tris-buffered saline [20 mM Tris (pH 8.0) and 150 mM NaCl] supplemented with 0.1 mM EDTA. Discoidal rHDL was prepared by the cholate dialysis method [47,48]. Briefly, 1-palmitoyl-2-oleoyl-*sn*-glycero-3-phosphocholine (POPC), free cholesterol (FC) and ApoA-I were combined at a molar ratio of 100:5:1. POPC and FC were dissolved in chloroform/methanol (2:1, v/v), and the organic solvents were evaporated under a stream of N2. The resulting lipid film was suspended with sodium deoxycholate at the deoxycholate/POPC molar ratio of 2:1 and incubated at −20 °C (2–4 h) and at 4 °C until the solution becomes clear. Purified ApoA-I was solubilized in 3 M guanidine HCl and added to the POPC/FC suspension at a POPC/ApoA-I molar ratio of 100:1. The resulting POPC/FC/ApoA-I mixture was incubated for 30 min at room temperature and then dialyzed extensively against Tris-buffered saline. The concentration of rHDL was determined based on the ApoA-I concentration, assuming an ApoA-I/rHDL ratio of 2:1 [5,47].

Cell-free expression

Cell-free reactions were performed as previously described [49,50] with minor changes. Briefly, the reactions were set up in a 35-µl batch volume with 2-h incubation at 30 °C. The reaction mixture contained the template DNA (i.e., G3C9 PON1's gene and its mutants in a modified pET32b plasmid [44]) at 8–10 ng/µl, 12.3 µl *E. coli* S30 extract [49], 0.3 U/µl RiboLock RNase inhibitor, 0.05 U/µl T7-RNA polymerase, 0.5 mg/ml tRNA *E. coli*, 0.04 mg/ml pyruvate kinase, 0.55 mM amino acid mix (RCWMDE was added in 1 mM concentration), 20 mM acetyl phosphate lithium potassium salt (pH 7), 20 mM phosphoenolpyruvate (monopotassium salt, pH 7), NTP mix (as described in Ref. [49]), 2 mM 1,4-dithiothreitol, 0.1 mg/ml folinic acid, 1× complete protease inhibitor cocktail (Roche), Hepes–EDTA buffer (as described in Ref. [49]), 9 mM magnesium acetate tetrahydrate, 130 mM potassium acetate, 2% polyethylene glycol 8000 and 0.05% sodium azide. The cell-free reactions were supplemented with rHDL at concentrations ranging from 0 to 10 µM.

Stimulation of PON1 lactonase activity by rHDL

The lactonase activity stimulation of PON1 by rHDL was measured as previously described [5,6], with some minor changes. Briefly, the cell-free products of G3C9-PON1 at different rHDL concentrations were diluted (1:50) into activity buffer and assayed with TBBL (0.25 mM). The resulting lactonase activity was compared to that of the cell-free product of G3C9-PON1 in the absence of rHDL. Data were fitted to the Langmuir saturation curve $\{V = v_{max}(\text{rHDL})/[(\text{rHDL}) + K_{app}] + 100\}$, from which the maximal stimulation levels (v_{max}) and the apparent affinity (K_{app}, concentration of rHDL particles required for 50% stimulation) were derived.

Inactivation of re-PON1 by calcium chelation

Cell-free products of G3C9-PON1 containing 10 µM rHDL were mixed with an equal volume of inactivation buffer [30 mM EDTA in 50 mM Tris (pH 8)] and incubated at 37 °C. After 72 h, aliquots from the inactivation mixture reactions were diluted (1:40) into activity buffer and the residual lactonase activity was determined with 0.5 mM TBBL.

Conformational sampling of PON1 by normal mode analysis

The conformational space of PON1 was explored by normal mode analysis. To calculate the normal modes, we used the ElNémo server[†] [51]. As input, we used both the free and the complex structures of PON1 [22] (PDB codes 3SRG and 3SRE, respectively). The following ElNémo default values were applied: NMODES 5, DQMIN 100, DQMAX 100, DQSTEP 20. The output comprised five coordinate files representing the five lowest-frequency modes. Structural analyses and figures were performed with PyMOL [52].

Computational modeling of the catalytic step

All EVB calculations were performed using the Q simulation package [53] and the OPLS-AA force field [54]. Paraoxon and TBBL hydrolyses were simulated starting from a crystal structure of PON1 in complex with an inhibitor (PDB code 3SRG) and snapshots showing large H2 displacements along the first five non-trivial normal modes obtained from analysis with ElNémo. Specifically, a "trivial" normal mode is a normal mode with a zero frequency (corresponding to a stationary system). The system possesses six trivial/zero frequencies, which correspond to the three overall rotations and three translations of the system. All other normal modes are referred to as "non-trivial", and the structures selected as starting points for subsequent EVB simulations were taken from projections along these normal modes showing

the largest displacements of the H2 helix. The K192Q mutation was subsequently performed manually for each structure using the Richardson [55] library as implemented in Chimera [56], in order to be able to directly compare wild-type and mutant PON1 conformations from the normal mode analysis for different substrates. In each case, the system was solvated using a 25-Å water sphere and the structures were gradually heated from 0 to 300 K over the course of 1 ns, followed by 5.375 ns initial MD equilibration on the initial structure for each system. Fifteen snapshots were obtained from the last 375 ps of the MD equilibration and were used as starting points for subsequent EVB simulations. The EVB simulations were 10.2 ns in length for each of 15 replicas for each system, leading to a total of 3.672 μs of EVB simulations over all systems and replicas (including the relevant background reactions). A more extensive description of the simulation setup and a download link to all relevant EVB parameters is provided in the supporting information.

Crystallization, data collection and refinement

The purest fractions of the G2E6 PON1-K192Q as judged by SDS PAGE were concentrated to 10–20 mg/ml and crystallized as previously described [22,23]. A complete data set was collected on beamline ID-14-4 at the European Synchrotron Radiation Facility Synchrotron (Grenoble, France). The diffraction images were indexed, integrated and scaled using the HKL2000 program package [57]. Structure determination was carried out by molecular replacement (Phaser and CCP4 [58]) using the published pH 6.5 structure (PDB code 3SRE) as a model. All steps of atomic refinement were carried out with CCP4/Refmac5 [59]. The model was built into $2F_o - F_c$ and $F_o - F_c$ maps using the program Coot [60]. As for previously obtained PON1 structures, this mutant does not display well-defined electron density for both the N-terminal helix (first ~20 residues) and the active-site flexible loop (residues 70–81), as well as contains one molecule of DDM (only the sugar moiety). Details of data collection and refinement statistics are displayed in Table S5. Figures depicting structures were prepared using PyMOL [52]. Coordinates and structure factors of the PON1-K192Q mutant have been deposited in the PDB under the accession number 4Q1U.

Accession numbers

Coordinates and structure factors of the K192Q mutant have been deposited in the Protein Data Bank under accession number 4Q1U.

Acknowledgements

We thank the Israel Structural Proteomics Centre for access to their protein purification and crystallization facilities. We also thank Tamar Unger and Erik Henrich for their valuable assistance in setting up the cell-free experiments. Financial supports by the Adelis Foundation, National Institute of Health (2-U54-NS058183), Defense Threat Reduction Agency (HDTRA1-11-C-0026) and the Benoziyo Center for Neuroscience are gratefully acknowledged. D.S.T. is the Nella and Leon Benoziyo Professor of Biochemistry. J.L.S. is the Pickman Professor of Structural Biology. S.C.L.K. would also like to thank the Swedish Research Council and the Knut and Alice Wallenberg Foundation for funding and support (VR grant 2010-5026 and a Wallenberg Academy Fellowship, respectively). All simulations were performed on the Triolith Cluster at National Supercomputer Centre in Linköping, Sweden, and the Abisko Cluster at High Performance Computing Center North in Umeå, through the Swedish National Infrastructure for Computing grant SNIC2013-26-1.

Appendix A. Supplementary data

Supplementary data to this article can be found online at http://dx.doi.org/10.1016/j.jmb.2015.01.013.

Received 31 October 2014;
Received in revised form 20 January 2015;
Accepted 22 January 2015
Available online 30 January 2015

Keywords:
PON1;
192 polymorphism;
interfacial activation;
enzyme dynamics;
HDL

†http://igs-server.cnrs-mrs.fr/elnemo/.

Abbreviations used:
HDL, high-density lipoprotein; ApoA-I, apolipoprotein A-I; DDM, *n*-dodecyl-β-D-maltoside; EDTA, ethylenediaminetetraacetic acid; EVB, empirical valence bond; MD, molecular dynamics; POPC, 1-palmitoyl-2-oleoyl-*sn*-glycero-3-phosphocholine; FC, free cholesterol.

References

[1] Bandeali S, Farmer J. High-density lipoprotein and atherosclerosis: the role of antioxidant activity. Curr Atheroscler Rep 2012;14:101–7.
[2] Lund-Katz S, Phillips MC. High density lipoprotein structure–function and role in reverse cholesterol transport. Subcell Biochem 2010;51:183–227.
[3] Huang Y, Wu Z, Riwanto M, Gao S, Levison BS, Gu X, et al. Myeloperoxidase, paraoxonase-1, and HDL form a functional ternary complex. J Clin Invest 2013;123:3815–28.
[4] Blatter MC, James RW, Messmer S, Barja F, Pometta D. Identification of a distinct human high-density lipoprotein subspecies defined by a lipoprotein-associated protein, K-45.

Identity of K-45 with paraoxonase. Eur J Biochem 1993;211: 871–9.
[5] Gaidukov L, Tawfik DS. High affinity, stability, and lactonase activity of serum paraoxonase PON1 anchored on HDL with ApoA-I. Biochemistry 2005;44:11843–54.
[6] Gaidukov L, Viji RI, Yacobson S, Rosenblat M, Aviram M, Tawfik DS. ApoE induces serum paraoxonase PON1 activity and stability similar to ApoA-I. Biochemistry 2010;49:532–8.
[7] Aviram M, Vaya J. Paraoxonase 1 activities, regulation, and interactions with atherosclerotic lesion. Curr Opin Lipidol 2013;24:339–44.
[8] Shih DM, Gu L, Xia YR, Navab M, Li WF, Hama S, et al. Mice lacking serum paraoxonase are susceptible to organophosphate toxicity and atherosclerosis. Nature 1998;394:284–7.
[9] Gaidukov L, Rosenblat M, Aviram M, Tawfik DS. The 192R/Q polymorphs of serum paraoxonase PON1 differ in HDL binding, lipolactonase stimulation, and cholesterol efflux. J Lipid Res 2006;47:2492–502.
[10] Almen MS, Nordstrom KJ, Fredriksson R, Schioth HB. Mapping the human membrane proteome: a majority of the human membrane proteins can be classified according to function and evolutionary origin. BMC Biol 2009;7:50.
[11] Brzozowski AM, Derewenda U, Derewenda ZS, Dodson GG, Lawson DM, Turkenburg JP, et al. A model for interfacial activation in lipases from the structure of a fungal lipase-inhibitor complex. Nature 1991;351:491–4.
[12] van den Berg B, Tessari M, Boelens R, Dijkman R, de Haas GH, Kaptein R, et al. NMR structures of phospholipase A2 reveal conformational changes during interfacial activation. Nat Struct Biol 1995;2:402–6.
[13] Harel M, Aharoni A, Gaidukov L, Brumshtein B, Khersonsky O, Meged R, et al. Structure and evolution of the serum paraoxonase family of detoxifying and anti-atherosclerotic enzymes. Nat Struct Mol Biol 2004;11:412–9.
[14] Reetz MT, Soni P, Fernandez L. Knowledge-guided laboratory evolution of protein thermolability. Biotechnol Bioeng 2009; 102:1712–7.
[15] Spiller B, Gershenson A, Arnold FH, Stevens RC. A structural view of evolutionary divergence. Proc Natl Acad Sci U S A 1999;96:12305–10.
[16] Zavodszky P, Kardos J, Svingor A, Petsko GA. Adjustment of conformational flexibility is a key event in the thermal adaptation of proteins. Proc Natl Acad Sci U S A 1998;95:7406–11.
[17] Oda MN, Bielicki JK, Berger T, Forte TM. Cysteine substitutions in apolipoprotein A-I primary structure modulate paraoxonase activity. Biochemistry 2001;40:1710–8.
[18] Bar-Rogovsky H, Hugenmatter A, Tawfik DS. The evolutionary origins of detoxifying enzymes: the mammalian serum paraoxonases (PONs) relate to bacterial homoserine lactonases. J Biol Chem 2013;288:23914–27.
[19] Yeung DT, Lenz DE, Cerasoli DM. Human paraoxonase I: A potential bioscavenger of organophosphorus nerve agents. The Paraoxonases: Their Role in Disease Development and Xenobiotic Metabolism. Dordrecht, The Netherlands: Springer; 2008. p. 151–70.
[20] Josse D, Xie W, Renault F, Rochu D, Schopfer LM, Masson P, et al. Identification of residues essential for human paraoxonase (PON1) arylesterase/organophosphatase activities. Biochemistry 1999;38:2816–25.
[21] Khersonsky O, Tawfik DS. The histidine 115-histidine 134 dyad mediates the lactonase activity of mammalian serum paraoxonases. J Biol Chem 2006;281:7649–56.
[22] Ben-David M, Elias M, Filippi JJ, Dunach E, Silman I, Sussman JL, et al. Catalytic versatility and backups in enzyme active sites: the case of serum paraoxonase 1. J Mol Biol 2012;418: 181–96.
[23] Ben-David M, Wieczorek G, Elias M, Silman I, Sussman JL, Tawfik DS. Catalytic metal ion rearrangements underline promiscuity and evolvability of a metalloenzyme. J Mol Biol 2013;425:1028–38.
[24] Billecke S, Draganov D, Counsell R, Stetson P, Watson C, Hsu C, et al. Human serum paraoxonase (PON1) isozymes Q and R hydrolyze lactones and cyclic carbonate esters. Drug Metab Dispos 2000;28:1335–42.
[25] Kuo CL, La Du BN. Calcium binding by human and rabbit serum paraoxonases. Structural stability and enzymatic activity. Drug Metab Dispos 1998;26:653–60.
[26] Kamerlin SCL, Warshel A. The EVB as a quantitative tool for formulating simulations and analyzing biological and chemical reactions. Faraday Discuss 2010;145:71–106.
[27] Duarte F, Bauer P, Barrozo A, Amrein BA, Purg M, Åqvist J, et al. Force-field independent metal parameters using a nonbonded dummy model. J Phys Chem B 2014;118:4351–62.
[28] Kamerlin SC, Sharma PK, Prasad RB, Warshel A. Why nature really chose phosphate. Q Rev Biophys 2013;46:1–132.
[29] Sanan TT, Muthukrishnan S, Beck JM, Tao P, Hayes CJ, Otto TC, et al. Computational modeling of human paraoxonase 1: preparation of protein models, binding studies, and mechanistic insights. J Phys Org Chem 2010;23:357–69.
[30] Richard JP, Amyes TL, Goryanova B, Zhai X. Enzyme architecture: on the importance of being in a protein cage. Curr Opin Chem Biol 2014;21:1–10.
[31] Furlong CE, Cole TB, Jarvik GP, Pettan-Brewer C, Geiss GK, Richter RJ, et al. Role of paraoxonase (PON1) status in pesticide sensitivity: genetic and temporal determinants. Neurotoxicology 2005;26:651–9.
[32] Kuo CL, La Du BN. Comparison of purified human and rabbit serum paraoxonases. Drug Metab Dispos 1995;23:935–44.
[33] Sorenson RC, Bisgaier CL, Aviram M, Hsu C, Billecke S, La Du BN. Human serum paraoxonase/arylesterase's retained hydrophobic N-terminal leader sequence associates with HDLs by binding phospholipids: apolipoprotein A-I stabilizes activity. Arterioscler Thromb Vasc Biol 1999;19:2214–25.
[34] Burke JE, Dennis EA. Phospholipase A2 structure/function, mechanism, and signaling. J Lipid Res 2009;50:S237–42.
[35] Qin S, Pande AH, Nemec KN, Tatulian SA. The N-terminal alpha-helix of pancreatic phospholipase A2 determines productive-mode orientation of the enzyme at the membrane surface. J Mol Biol 2004;344:71–89.
[36] Chiou YL, Cheng YC, Kao PH, Wang JJ, Chang LS. Mutations on the N-terminal region abolish differentially the enzymatic activity, membrane-damaging activity and cytotoxicity of Taiwan cobra phospholipase A2. Toxicon 2008;51: 270–9.
[37] Chiou YL, Lin SR, Chang LS. Mutations on N-terminal region of Taiwan cobra phospholipase A(2) result in structurally distorted effects. J Pept Sci 2008;14:890–7.
[38] Berg OG, Gelb MH, Tsai MD, Jain MK. Interfacial enzymology: the secreted phospholipase A(2)-paradigm. Chem Rev 2001;101:2613–54.
[39] Seeger F, Quintyn R, Tanimoto A, Williams GJ, Tainer JA, Wysocki VH, et al. Interfacial residues promote an optimal alignment of the catalytic center in human soluble guanylate cyclase: heterodimerization is required but not sufficient for activity. Biochemistry 2014;53:2153–65.
[40] Elias M, Wieczorek G, Rosenne S, Tawfik DS. The universality of enzymatic rate-temperature dependency. Trends Biochem Sci 2014;39:1–7.

[41] Giger L, Caner S, Obexer R, Kast P, Baker D, Ban N, et al. Evolution of a designed retro-aldolase leads to complete active site remodeling. Nat Chem Biol 2013;9:494–8.
[42] Khersonsky O, Kiss G, Rothlisberger D, Dym O, Albeck S, Houk KN, et al. Bridging the gaps in design methodologies by evolutionary optimization of the stability and proficiency of designed Kemp eliminase KE59. Proc Natl Acad Sci U S A 2012;109:10358–63.
[43] Preiswerk N, Beck T, Schulz JD, Milovnik P, Mayer C, Siegel JB, et al. Impact of scaffold rigidity on the design and evolution of an artificial Diels-Alderase. Proc Natl Acad Sci U S A 2014;111:8013–8.
[44] Aharoni A, Gaidukov L, Yagur S, Toker L, Silman I, Tawfik DS. Directed evolution of mammalian paraoxonases PON1 and PON3 for bacterial expression and catalytic specialization. Proc Natl Acad Sci U S A 2004;101:482–7.
[45] Erijman A, Dantes A, Bernheim R, Shifman JM, Peleg Y. Transfer-PCR (TPCR): a highway for DNA cloning and protein engineering. J Struct Biol 2011;175:171–7.
[46] Ryan RO, Forte TM, Oda MN. Optimized bacterial expression of human apolipoprotein A-I. Protein Expr Purif 2003;27:98–103.
[47] Matz CE, Jonas A. Micellar complexes of human apolipoprotein A-I with phosphatidylcholines and cholesterol prepared from cholate-lipid dispersions. J Biol Chem 1982;257:4535–40.
[48] Nichols AV, Gong EL, Blanche PJ, Forte TM. Characterization of discoidal complexes of phosphatidylcholine, apolipoprotein A-I and cholesterol by gradient gel electrophoresis. Biochim Biophys Acta 1983;750:353–64.
[49] Schneider B, Junge F, Shirokov VA, Durst F, Schwarz D, Dotsch V, et al. Membrane protein expression in cell-free systems. Methods Mol Biol 2010;601:165–86.
[50] Schwarz D, Junge F, Durst F, Frolich N, Schneider B, Reckel S, et al. Preparative scale expression of membrane proteins in *Escherichia coli*-based continuous exchange cell-free systems. Nat Protoc 2007;2:2945–57.
[51] Suhre K, Sanejouand YH. ElNémo: a normal mode web server for protein movement analysis and the generation of templates for molecular replacement. Nucleic Acids Res 2004;32:W610–4.
[52] DeLano WL. "The PyMOL Molecular Graphics System". CA, USA: DeLano Scientific LLC. San Carlos; 2002 http://www.pymol.org.
[53] Marelius J, Kolmodin K, Feierberg I, Åqvist J. Q: a molecular dynamics program for free energy calculations and empirical valence bond simulations in biomolecular systems. J Mol Graph Model 1998;16:261.
[54] Jorgensen WL, Maxwell DS, Tirado-Rives J. Development and testing of the OPLS all-atom force field on conformational energetics and properties of organic liquids. J Am Chem Soc 1996;118:11225–36.
[55] Lovell SC, Word JM, Richardson JS, Richardson DC. The penultimate rotamer library. Proteins 2000;40:389–408.
[56] Pettersen EF, Goddard TD, Huang CC, Couch GS, Greenblatt DM, Meng EC, et al. UCSF Chimera—a visualization system for exploratory research and analysis. J Comput Chem 2004;25:1605–12.
[57] Otwinowski Z, Minor W. Processing of X-ray diffraction data collected in oscillation mode. Methods Enzymol 1997;276:307–26.
[58] McCoy AJ, Grosse-Kunstleve RW, Adams PD, Winn MD, Storoni LC, Read RJ. Phaser crystallographic software. J Appl Crystallogr 2007;40:658–74.
[59] Murshudov GN, Vagin AA, Dodson EJ. Refinement of macromolecular structures by the maximum-likelihood method. Acta Crystallogr D Biol Crystallogr 1997;53:240–55.
[60] Emsley P, Cowtan K. Coot: model-building tools for molecular graphics. Acta Crystallogr D Biol Crystallogr 2004;60:2126–32.